Published in final edited form as:
J Mol Biol. 2012 February 10; 416(1): 57–77. doi:10.1016/j.jmb.2011.12.015.

Ligand Binding and Membrane Insertion Compete with Oligomerization of the BclXL Apoptotic Repressor

Vikas Bhat[1], **Caleb B. McDonald**[1], **David C. Mikles**[1], **Brian J. Deegan**[1], **Kenneth L. Seldeen**[1], **Margaret L. Bates**[2], and **Amjad Farooq**[1,*]

[1]Department of Biochemistry & Molecular Biology and USylvester Braman Family Breast Cancer Institute, Leonard Miller School of Medicine, University of Miami, Miami, FL 33136

[2]The Miami Project to Cure Paralysis, Leonard Miller School of Medicine, University of Miami, Miami, FL 33136

Abstract

BclXL apoptotic repressor plays a central role in determining the fate of cells to live or die during physiological processes such as embryonic development and tissue homeostasis. Herein, using a myriad of biophysical techniques, we provide evidence that ligand binding and membrane insertion compete with oligomerization of BclXL in solution. Of particular importance is the observation that such oligomerization is driven by the intermolecular binding of its C-terminal transmembrane (TM) domain to the canonical hydrophobic groove in a domain-swapped trans-fashion, whereby the TM domain of one monomer occupies the canonical hydrophobic groove within the other monomer and vice versa. Binding of BH3 ligands to the canonical hydrophobic groove displaces the TM domain in a competitive manner allowing BclXL to dissociate into monomers upon hetero-association. Remarkably, spontaneous insertion of BclXL into DMPC/DHPC bicelles results in a dramatic conformational change such that it can no longer recognize the BH3 ligands in what has come to be known as the “hit-and-run” mechanism. Collectively, our data suggest that oligomerization of a key apoptotic repressor serves as an allosteric switch that fine tunes its ligand binding and membrane insertion pertinent to the regulation of apoptotic machinery.

Keywords

BclXL apoptotic repressor; Protein oligomerization; Ligand binding; Membrane insertion; Allosteric regulation

INTRODUCTION

Apoptosis plays a key role in removing damaged and unwanted cells in a highly programmed and coordinated manner during physiological processes such as embryonic development and tissue homeostasis. Importantly, deregulation of apoptotic machinery can result in the development of diseases such as cancer and neurodegenerative disorders [1–3]. The Bcl2 family of proteins has come to be regarded as a central player in coupling apoptotic stimuli to determining the fate of cells to live or die [4–11]. The Bcl2 proteins can be divided into three major groups: activators, effectors and repressors. Activators such as Bid and Bad belong to the BH3-only proteins, where BH3 is the Bcl2 homology 3 domain. Effectors such as Bax and Bak contain the BH3-BH1-BH2-TM modular architecture, where

*To whom correspondence should be addressed: amjad@farooqlab.net, tel 305-243-2429, fax 305-243-3955.

TM is the transmembrane domain located C-terminal to Bcl2 homology domains BH3, BH1 and BH2. Repressors such as Bcl2, BclXL and BclW are characterized by the BH4-BH3-BH1-BH2-TM modular organization, with an additional N-terminal Bcl2 homology 4 domain.

According to one school of thought, the apoptotic fate, or the decision of a cell to continue to live or pull the trigger to commit suicide, is determined by the cellular ratio of activator, effector and repressor molecules [12; 13]. In quiescent and healthy cells, the effectors are maintained in an inactive state via complexation with repressors. Upon receiving apoptotic cues, in the form of DNA damage and cellular stress, the activators are stimulated and compete with effectors for binding to the repressors and, in so doing, not only do they neutralize the anti-apoptotic action of repressors but also unleash the pro-apoptogenicity of effectors. The effectors subsequently initiate apoptotic cell death by virtue of their ability to insert into the mitochondrial outer membrane (MOM) resulting in the formation of mitochondrial pores in a manner akin to the insertion of bacterial toxins such as colicins and diphtheria [14–18]. In addition to freeing up the effectors from the inhibitory effect of repressors, the activators are also believed to directly bind to effectors and facilitate their participation in the assembly of mitochondrial pores. This provides a route for the release of apoptogenic factors such as cytochrome c and Smac/Diablo from mitochondria into the cytosol. Subsequently, rising levels of apoptogenic factors in the cytosol switch on aspartate-specific proteases termed caspases, which in turn, demolish the cellular architecture by cleavage of proteins culminating in total cellular destruction. Importantly, studies suggest that the release of apoptogenic factors may occur through the so-called voltage-dependent anion channel (VDAC) located within MOM [19]. Thus, while apoptotic effectors such as Bax and Bak accelerate the opening of VDAC, apoptotic repressors such as BclXL and Bcl2 have been shown to trigger its closing. Although the precise mechanism of how exactly various members of the Bcl2 family execute and regulate apoptosis remains a subject of immense controversy, it is generally agreed that hetero-association between various members of the Bcl2 family is one of the defining events in the decision of a cell to live or die.

Despite their low sequence convergence, all members of Bcl2 family share a remarkably conserved 3D topological fold characterized by a central predominantly hydrophobic α-helical hairpin “dagger” (α5 and α6) surrounded by a “cloak” comprised of six amphipathic α-helices (α1–α4 and α7–α8) of varying lengths [20]. Additionally, the effectors and repressors also contain a C-terminal hydrophobicα-helix termed α9, or more commonly the TM domain, because it allows these members of the Bcl2 family to localize to MOM upon apoptotic induction [21–23]. The “cloak and dagger” structural topology of Bcl2 members is the hallmark of their functional duality in that they are able to co-exist as “soluble factors” under quiescent cellular state and as “membrane channels” upon apoptotic induction. Notably, the hydrophobic dagger not only provides the bulk of the thermodynamic force in driving the water-membrane transition of various Bcl2 members upon apoptotic induction but also directly participates in the formation of mitochondrial pores that provide a smooth channel for the exit of apoptogenic factors. A prominent feature of repressors is that they contain what has come to be known as the “canonical hydrophobic groove”, formed by the juxtaposition of α2–α5 helices, that serves as the docking site for the BH3 domain (α2 helix) of activators and effectors. In a remarkable twist, the effectors also contain a hydrophobic groove for accommodating the BH3 domain of activators but this “pseudo hydrophobic groove”, formed by the juxtaposition of α1/α6 helices, is geographically distinct in that it is located on the face opposite to that occupied by the canonical hydrophobic groove in repressors [24–26]. Surprisingly, in the case of Bax effector, the canonical hydrophobic groove is occupied by its C-terminal TM domain (α9 helix) in an intramolecular manner [27]. The binding of activators via their BH3 domains to the pseudo hydrophobic groove within Bax is

believed to disengage the TM domain allowing it to translocate to MOM in response to apoptotic signals [24–26]. In a manner akin to the autoinhibition of Bax for mitochondrial translocation [27], the canonical hydrophobic groove within the BclW repressor is also not freely available but rather locked down through intramolecular binding of its TM domain (α9 helix) [28; 29]. Subsequent binding of the BH3 domain of activators and effectors to the canonical hydrophobic groove within BclW is believed to displace the TM domain so as to allow it to translocate to MOM upon apoptotic induction and, in so doing, neutralize its anti-apoptotic activity [30].

In an effort to further understand how the TM domain and MOM modulate the binding of BH3 ligands to repressors, we set out here to analyze biophysical properties of full-length BclXL construct (BclXL_FL) and a truncated BclXL construct (BclXL_dTM) in which the TM domain has been deleted alone and their behaviors toward BH3 ligands in solution and in DMPC/DHPC bicelles mimicking MOM (Figure 1). Our study reveals that ligand binding and membrane insertion compete with oligomerization of BclXL in solution. Of particular importance is the observation that such oligomerization is driven by the intermolecular binding of its C-terminal transmembrane (TM) domain to the canonical hydrophobic groove in a domain-swapped trans-fashion, whereby the TM domain of one monomer occupies the canonical hydrophobic groove within the other monomer and vice versa. Binding of BH3 ligands to the canonical hydrophobic groove displaces the TM domain in a competitive manner allowing BclXL to dissociate into monomers upon hetero-association. Remarkably, spontaneous insertion of BclXL into DMPC/DHPC bicelles results in a dramatic conformational change such that it can no longer recognize the BH3 ligands in what has come to be known as the “hit-and-run” mechanism. Collectively, our data suggest that oligomerization of a key apoptotic repressor serves as an allosteric switch that fine tunes its ligand binding and membrane insertion pertinent to the regulation of apoptotic machinery.

RESULTS and DISCUSSION

TM modulates the binding of BH3 ligands to BclXL

To shed light on the role of TM domain in modulating the binding of BH3 ligands to BclXL, we conducted ITC analysis on BclXL_FL and BclXL_dTM constructs using BH3 peptides derived from Bid and Bad activators and the Bax effector — the three well-characterized physiological ligands of BclXL repressor [9–11]. Figure 2 provides representative ITC data for the binding of Bid_BH3 peptide to BclXL_FL and BclXL_dTM constructs, while detailed thermodynamic parameters accompanying the binding of all BH3 peptides are shown in Table 1. It is evident from our data that the BH3 peptides bind to the BclXL_dTM construct with affinities that are more than an order of magnitude greater than those observed for their binding to the BclXL_FL construct. That this is so strongly suggests that the TM domain in BclXL is not freely exposed to solution but rather associates with the rest of the protein in a manner that inhibits the binding of BH3 ligands. In light of the knowledge that the TM domain of BclW repressor occupies the canonical hydrophobic groove [28–30], it can be argued that a similar scenario prevails in the case of BclXL and that the binding of BH3 ligands competes with the dissociation of TM domain from the canonical hydrophobic groove.

In addition to dramatic differences observed in the binding affinities of various BH3 peptides toward BclXL_FL and BclXL_dTM constructs, their intermolecular association is also marked by distinct underlying thermodynamic forces. Thus, while binding of various BH3 ligands to BclXL_FL construct is predominantly driven by favorable enthalpic factors accompanied by entropic penalty, binding to BclXL_dTM construct is favored by both enthalpic and entropic changes (Table 1). These salient observations indicate that the solvation of hydrophobic TM domain following the recruitment of BH3 ligands by the

canonical hydrophobic groove most likely mitigates the conformational entropy of BclXL. We believe that such loss in conformational dynamics may aid or prime BclXL for subsequent insertion into MOM so as to allow it to interfere with the formation of mitochondrial pores critical for the release of apoptogenic factors into the cytosol. Our data exquisitely illustrate how thermodynamics may gauge the decision of a cell to live or die. Importantly, previous studies suggest that upon insertion into MOM, repressors undergo substantial conformational change and lose their ability to hold onto BH3 ligands in what has been termed the "hit-and-run" mechanism [29; 31–33]. To test the validity of this hypothesis further, we also measured the binding of various BH3 peptides to BclXL_FL and BclXL_dTM constructs pre-equilibrated with DMPC/DHPC bicelles as a mimetic for MOM using ITC (Figure 2). Our data reveal that the BH3 peptides do not recognize BclXL within bicelles in the presence or absence of TM domain and thereby further corroborate the hit-and-run model of the binding of repressors to their BH3 ligands preceding their insertion into MOM.

Given that we have relied here on isolated BH3 peptides to mimic intact Bid, Bad and Bax, caution is warranted in that the BH3 domains may depart from their physiological behavior when treated as isolated peptides due to the loss of local conformational constraints that they may be subject to in the context of full-length proteins. Nonetheless, it is well-documented that Bid, Bad and Bax interact with apoptotic repressors primarily through their BH3 domains. Additionally, binding of BH3 peptides to apoptotic repressors with high-affinity and specificity as observed here and elsewhere argues strongly in support of BH3 peptides as bona fide models of intact proteins from which they are derived [34–36]. We also note that the BH3 domain of Bid binds to apoptotic repressors only upon cleavage of N-terminal region of the protein [37]. In short, the use of isolated BH3 peptides here in lieu of full-length proteins is well-justified and our data presented above are likely to be of physiological relevance.

BclXL associates into higher-order oligomers

Our data presented above suggest strongly that the TM domain competes with the binding of BH3 ligands by virtue of its ability to bind to the canonical hydrophobic groove. However, unlike the association of TM domain of BclW repressor and Bax effector via an intramolecular cis-fashion [27–29], the possibility that the TM domain of BclXL may associate in an intermolecular trans-fashion so as to form domain-swapped dimers cannot be excluded. To test this notion, we next conducted ALS analysis on BclXL_FL and BclXL_dTM constructs and quantified various physical parameters accompanying the behavior of these protein constructs in solution from the first principles of hydrodynamics without any assumptions (Figure 3 and Table 2). Remarkably, our data show that while BclXL_FL construct predominantly associates into higher-order oligomers that we herein refer to as multimer (~300kD) and polymer (~3000kD), the BclXL_dTM construct is largely monomeric in solution. That this is so strongly implicates the involvement of TM domain in mediating the formation of domain-swapped dimers of BclXL_FL that further associate into larger oligomeric species. In light of our ITC data presented above, we believe that such oligomerization likely serves as an auto-inhibitory allosteric switch under quiescent cellular state. However, upon the induction of apoptosis, the rising cellular levels of BH3 ligands in the form of activators compete with oligomerization of BclXL so as to dislodge the TM domain from the canonical hydrophobic groove and thereby initiating its translocation into MOM — a key requisite for its anti-apoptotic behavior. Although a minor fraction of both BclXL_FL and BclXL_dTM constructs is also observed as a dimer, we believe that these homodimers are physically-distinct. BclXL_FL dimer is most likely constructed through TM-swapping, such that the TM domain of one monomer occupies the canonical hydrophobic groove within the other monomer and vice versa in an intermolecular trans-

fashion, in agreement with our observations that the binding of BH3 ligands to the canonical hydrophobic groove is compromised in the context of full-length BclXL (Table 1). This notion is also consistent with previous studies in which the TM domain was shown to promote homodimerization of full-length BclXL within live cells [32; 38]. In contrast, the formation of BclXL_dTM dimer is most probably driven through inter-monomer swapping of α6–α8 helices such that the canonical hydrophobic grooves within each monomer remain fully exposed to solution and are available for the binding of BH3 ligands without any restriction as reported earlier in the case of BclXL and BclW constructs in which the TM domain has been truncated [39–41].

It should also be noted here that when SEC-resolved fractions containing the BclXL_FL monomer and dimer were re-analyzed on SEC column, both the oligomeric species re-appeared in the elution profile. Likewise, re-analysis of SEC-resolved fractions containing the BclXL_FL higher-order oligomers on SEC column also resulted in the appearance of monomeric and dimeric species. Taken collectively, these salient observations suggest strongly that BclXL_FL exists in a reversible monomer-dimer-multimer-polymer equilibrium. The fact that such equilibrium prevails even at lower concentrations of BclXL argues strongly that the ability of BclXL to undergo oligomerization in solution is likely to be physiologically-relevant. In an attempt to gain insights into the conformational heterogeneity of the oligomeric species of BclXL, we also determined the M_w/M_n and R_g/R_h ratios from our hydrodynamic data (Table 2). While the M_w/M_n ratio provides a measure of the macromolecular polydispersity, the R_g/R_h ratio sheds light on the overall macromolecular shape. Our data suggest that while the higher-order oligomers of BclXL display some degree of polydispersity ($M_w/M_n > 1.05$), the monomeric and dimeric forms of BclXL are predominantly monodisperse ($M_w/M_n < 1.05$). Additionally, the higher-order oligomers of BclXL most likely adopt an elongated rod-like shape ($R_g/R_h > 1$) in lieu of a more spherical or disc-like architecture. That this is so was further confirmed by TEM analysis (Figure 4). Thus, while BclXL_FL alone exudes rod-like appearance in solution, addition of Bid_BH3 peptide is concomitant with the disappearance of these rod-like structures, implying that ligand binding most likely results in the dissociation of higher-order oligomers into monomers in agreement with our ITC data.

Ligand binding and membrane insertion modulate thermodynamic stability of BclXL

In light of our data presented above, we next wondered whether the ability of full-length BclXL to associate into higher-order oligomeric species is a manifestation of its enhanced stability and to what extent such thermodynamic advantage may be modulated by ligand binding and membrane insertion. Toward this goal, we conducted DSC analysis on BclXL_FL and BclXL_dTM constructs alone, in the presence of Bid_BH3 peptide and in the presence of DMPC/DHPC bicelles (Figure 5). Our analysis suggests that BclXL_FL is significantly more stable than BclXL_dTM. Thus, while the unfolding of BclXL_dTM is accompanied by a melting temperature (T_m) of 72°C, unfolding of BclXL_FL is not observed even when the melting temperature is raised to 120°C (Figures 5a and 5b). Addition of Bid_BH3 peptide to BclXL_dTM construct raises its T_m value to 78°C, implying that ligand binding enhances the stability of BclXL. In light of our ITC and TEM analysis, binding of BH3 peptide to BclXL_FL might be expected to destabilize this construct. Yet, no thermal melting of liganded BclXL_FL construct is observed in the 40–120°C temperature range in a manner akin to the unliganded BclXL_FL construct. This observation suggests that the liganded BclXL_FL construct is significantly more stable than liganded BclXL_dTM. Surprisingly, the behavior of BclXL_FL and BclXL_dTM constructs within bicelles is mirrored to that observed in solution. Thus, while no thermal melting of BclXL_dTM construct within bicelles is observed in the 40–120°C temperature range, the melting of BclXL_FL construct within bicelles is characterized by three distinct thermal

phases, with T_m values of 78°C, 89°C and 96°C. We attribute such multi-phasic thermal transition of BclXL_FL within bicelles to the dissociation of an higher-order oligomer into dimeric and monomeric species prior to melting. Notably, these observations are not affected when DSC analysis is conducted on BclXL_Fl construct at lower protein concentrations (Figure 5c), implying that the thermal behavior of BclXL within both solution and bicelles is likely to be of physiological relevance.

Taken collectively, our data suggest that although the BclXL_FL construct exists as an oligomer within bicelles, the physical basis of such oligomerization is likely to be distinct from that observed in solution and thereby supporting the notion that BclXL undergoes conformational change upon membrane insertion in agreement with previous reports [33; 42; 43]. Importantly, our data also suggest that although the BclXL_dTM construct is predominantly monomeric in solution, it undergoes oligomerization within bicelles to such an extent that it is stable up to a temperature of 120°C. This observation is in agreement with the view that the TM domain is not critical for the insertion of apoptotic repressors into membranes [33; 42; 44]. However, the observation that the BclXL_dTM oligomers within membranes are more stable than the BclXL_FL oligomers is being reported here for the first time. In light of this novel finding, we hypothesize that the TM domain may not only play a role in regulating ligand binding but that it may also control the degree of BclXL oligomerization within membranes. Importantly, it has been suggested that the TM domain targets BclXL to MOM as opposed to other intracellular membranes [45]. Thus, although the lack of TM domain may facilitate oligomerization of BclXL within membranes, the TM domain may play a key role in its correct intermembraneous localization as well as oligomerization relevant to its anti-apoptotic function.

BclXL undergoes tertiary and quaternary structural changes upon ligand binding and membrane insertion

It is believed that apoptotic repressors undergo substantial conformational changes upon insertion into membranes [33; 42]. In order to elucidate the role of TM domain in dictating such conformational changes within BclXL upon ligand binding and membrane insertion, we measured SSF spectra of BclXL_FL and BclXL_dTM constructs alone, in the presence of Bid_BH3 peptide and in the presence of DMPC/DHPC bicelles (Figure 6). It is important to note that intrinsic protein fluorescence, largely due to tryptophan residues, is influenced by changes in the local environment and thus serves as a sensitive probe of overall conformational changes within proteins. This is further aided by the fact that BclXL_FL and BclXL_dTM constructs respectively contain seven and six tryptophan residues positioned at various strategic positions to monitor conformational changes occurring at both the intramolecular and intermolecular level. Strikingly, our data show that the intrinsic fluorescence of BclXL_FL construct is much higher than that observed for the BclXL_dTM construct (Figures 6a and 6b). This most likely arises due to the interfacial burial of solvent-exposed tryptophans on the protein surface upon intermolecular association of BclXL_FL into higher-order oligomers. This is further evidence for the propensity of BclXL_FL construct to undergo oligomerization in solution.

Strikingly, although binding of Bid_BH3 peptide to both BclXL_FL and BclXL_dTM constructs results in the quenching of intrinsic fluorescence, the magnitude of such quenching is much larger for the BclXL_FL construct. These findings suggest that the binding of Bid_BH3 peptide to BclXL_FL construct is coupled to its dissociation into monomers, or in statistical terms, shifts the equilibrium in favor of monomers. In striking contrast to ligand binding, insertion of both BclXL_FL and BclXL_dTM constructs into bicelles results in the enhancement of intrinsic fluorescence in agreement with the overall movement of tryptophan residues from a polar environment to a more hydrophobic milieu. However, the extent of such fluorescence enhancement is much larger for the BclXL_FL

construct versus the BclXL_dTM construct. This implies that although both constructs undergo conformational changes upon insertion into bicelles, the BclXL_FL construct does so more dramatically and possibly resulting in its quaternary structural rearrangement in addition to tertiary structural changes. This salient observation thus further corroborates our DSC data where both BclXL_FL and BclXL_dTM constructs appear to form distinct oligomers within bicelles. Importantly, SEC-resolved fractions containing higher-order oligomers of BclXL_FL construct appear to behave very similar to non-resolved BclXL_FL in solution and within bicelles (Figures 6a and 6c), implying that the oligomers rapidly re-equilibrate in agreement with our ALS analysis.

BclXL undergoes secondary structural changes upon ligand binding and membrane insertion

To probe secondary structural changes upon ligand binding and membrane insertion, we next measured and compared far-UV CD spectra of BclXL_FL and BclXL_dTM constructs alone, in the presence of Bid_BH3 peptide and in the presence of DMPC/DHPC bicelles (Figure 7). Consistent with our SSF analysis above, both BclXL_FL and BclXL_dTM constructs display spectral features in the far-UV region characteristic of an α-helical-fold with bands centered around 208nm and 222nm (Figures 7a and 7b). Upon the addition of Bid_BH3 peptide, there is a noticeable increase in the far-UV spectral intensities of 208-nm and 222-nm bands within both constructs but more so in the case of BclXL_FL, implying that ligand binding is coupled to secondary structural changes. The nature of such increase in α-helicity is not clear but it is possible that this increase is in part due to the coil-helix transition of the BH3 peptide upon binding. Interestingly, the nature of secondary structural changes observed upon the addition of bicelles appears to be somewhat distinct to that observed upon ligand binding in both constructs. Thus, while the 208-nm band increases in intensity in the presence of bicelles, the 222-nm band undergoes reduction. Notably, SEC-resolved fractions containing the higher-order oligomers of BclXL_FL construct appear to behave very similar to non-resolved BclXL_FL in solution and within bicelles (Figures 7a and 7c), implying that the oligomers rapidly re-equilibrate in agreement with our ALS analysis. Taken together, our data suggest that ligand binding and membrane insertion of both BclXL_FL and BclXL_dTM constructs is coupled to secondary structural changes though the precise nature of such structural perturbations remains uncertain.

Structural models provide physical basis of oligomerization of BclXL

In an effort to understand the physical basis of oligomerization of full-length BclXL, we built 3D atomic models of BclXL monomers in which the TM domain is either exposed to solution (BclXL_solTM) or occupies the canonical hydrophobic groove (BclXL_cisTM) as well as the BclXL homodimer in which the TM domain of one monomer occupies the canonical hydrophobic groove within the other monomer and vice versa in a domain-swapped trans-fashion (BclXL_transTM) (Figure 8). It is noteworthy that these structural models were derived from the known solution structures of truncated BclXL, in which the TM domain and the α1–α2 loop are missing, and the full-length Bax in which the TM domain occupies the canonical hydrophobic groove [27; 46].

As discussed earlier, the topological fold of BclXL is comprised of a central predominantly hydrophobic α-helical hairpin dagger (α5 and α6) surrounded by a cloak comprised of six amphipathicα-helices (α1–α4 and α7–α8) of varying lengths. Additionally, the C-terminal hydrophobic TM domain (helix α9) may in principle adopt one of the following three conformations: The TM domain may be exposed to solution as depicted in the BclXL_solTM model (Figure 8a). However, given its predominantly hydrophobic nature, the TM domain is likely to become unfolded in solution while its association with the canonical hydrophobic groove, formed by the juxtaposition of α2–α5 helices, would be

thermodynamically favorable as shown in the BclXL_cisTM model (Figure 8b). Such an intramolecular association of TM domain has indeed been previously reported in the case of BclW repressor and Bax effector [27–29]. Disordered regions such as loops within proteins interconnecting αhelices or β-strands have come to prominence over the past decade or so in their ability to modulate protein structure and function [47–51]. Strikingly, the α8–α9 loop preceding the TM domain in BclXL is much longer than that found in Bax effector, while the anomalously long α1–α2 loop (~60 residues) in BclXL is relatively short in both the BclW repressor and the Bax effector. This raises the possibility that the TM domain in BclXL may not only associate with the rest of the protein in an intramolecular cis-manner but rather its intermolecular association in a trans-fashion through TM-swapping may be a preferred alternative as suggested by the BclXL_transTM model (Figure 8c). This latter notion is not only supported by cell-based studies on full-length BclXL [32; 38], but would also provide a physical route for the oligomerization of BclXL into higher-order oligomers reported here for the first time. Importantly, our BclXL_transTM model suggests that homodimerization, with the monomers related by a two-fold axis of symmetry, would lead to further thermodynamic stabilization of TM domains. Thus, roughly parallel orientation of TM domains within BclXL_transTM dimer would allow sidechain moieties of apolar residues facing outward from the TM domain within one monomer to engage in van der Waals contacts with sidechain moieties of apolar residues facing outward from the TM domain of the other monomer in a manner akin to hydrophobic interactions stabilizing leucine zippers [52]. Prevalence of such additional favorable interactions would clearly favor the docking of TM domain to the canonical hydrophobic groove via a trans-mechanism over intramolecular association.

MD simulations support dimerization of BclXL through domain-swapping

Our structural models of full-length BclXL presented above suggest strongly that the BclXL_transTM homodimeric conformation would be the most preferable in solution and, that the α1–α2 and α8–α9 loops may play an active role in driving such homodimerization. To further test the validity of our structural models and to gain insights into macromolecular dynamics, we next conducted MD simulations over tens of nanoseconds (Figure 9) — the time regime over which macromolecular motions such as conformational fluctuations and intermolecular movements relevant to their biological function occur. As shown in Figure 9a, the MD trajectories reveal that all three conformations of BclXL (BclXL_solTM, BclXL_cisTM and BclXL_transTM) reach structural equilibrium after about 20ns with an overall root mean square deviation (RMSD) between 5–10Å. To understand the rather low stability of these conformations, we deconvoluted the overall RMSD for the full-length (FL) BclXL spanning residues 1–233 into three constituent regions: (i) the central core (CC) region spanning residues 86–195; (ii) the N-terminal (NT) region, containing the α1 helix (BH4 domain) and the α1–α2 loop, spanning residues 1–85; and (iii) the C-terminal (CT) region, containing the α9 helix (TM domain) and the α8–α9 loop, spanning residues 196–233. To our surprise, we noticed that the overwhelming protein flexibility in all three conformations largely resides in the NT and CT regions, while the CC region displays a very high degree of order with little internal motions. However, the conformational dynamics of the NT and CT regions display discernable differences within the three distinct conformations of BclXL. In the case of BclXL_solTM conformation, both NT and CT regions remain highly mobile, reflecting in part the thermodynamically unfavorable solvation of the hydrophobic TM domain, which also appears to undergo unfolding during the course of MD trajectory. Interestingly, while the NT region remains relatively mobile in both BclXL_cisTM and BclXL_transTM conformations in a manner akin to its mobility observed within BclXL_solTM, the CT region experiences substantial loss of conformational dynamics which can be attributed to the stabilization of the TM domain by the canonical hydrophobic groove either in an intramolecular manner (BclXL_cisTM) or via

domain-swapping (BclXL_transTM). Importantly, the CT region appears to be less mobile and more ordered over the course of MD trajectory within BclXL_transTM relative to its mobility within the BclXL_cisTM conformation, arguing in favor of greater stability of homodimeric versus monomeric conformation.

An alternative means to assess mobility and stability of macromolecular complexes is through an assessment of the root mean square fluctuation (RMSF) of specific atoms over the course of MD simulation. Figure 9b provides such analysis for the backbone atoms of each residue within all three conformations of BclXL. In agreement with our RMSD analysis (Figure 9a), residues within the CC region appear to be the most ordered with least fluctuation. However, the RMSF analysis additionally reveals that the residues within NT and CT regions that undergo most fluctuation reside within the α1–α2 loop in all three conformations, while residues within theα8–α9 loop display higher mobility only in BclXL_solTM and BclXL_cisTM conformations. Remarkably, while the α8–α9 loop appears to be highly ordered in BclXL_transTM, the mobility of α1–α2 loop is comparatively much higher than that observed in BclXL_solTM and BclXL_cisTM conformations. It has also been previously shown that the deletion of the α1–α2 loop in BclXL augments its anti-apoptogenicity and that the suppressive effect of α1–α2 loop is relieved by its post-translational phosphorylation [53]. In light of this observation, we believe that the intrinsic flexibility of the α1–α2 loop may be a driving force for the homodimerization of BclXL through favorable entropic contributions and that such intermolecular association may provide a thermodynamic bottle-neck for it to switch to an active conformation. Post-translational phosphorylation of BclXL may induce conformational changes within the α1–α2 loop that lead to its ordering and thereby remove the bottle-neck promoting its homodimerization and subsequently shifting the equilibrium in favor of monomeric conformation that exudes higher anti-apoptogenicity.

Unlike the enhanced mobility of α1–α2 loop within BclXL_transTM, the ordering of the α8–α9 loop appears to provide a mechanism for greater stabilization of TM within BclXL_transTM compared to BclXL_cisTM conformation as evidenced by the RMSF of residues located within the TM domain (Figure 9b). Taken together, our MD simulations suggest that the dimeric BclXL_transTM conformation is more stable than either of the monomeric conformations and thereby further support the notion that domain-swapped homodimerization likely plays a key role in the intermolecular association of BclXL into higher-order oligomers.

CONCLUSIONS

Despite their discovery more than two decades ago [54–58], members of the Bcl2 family have not been extensively studied using biophysical tools. In particular, previous biophysical and structural studies on BclXL and Bcl2 repressors have heavily relied on truncated constructs devoid of both the structurally-disorderedα1–α2 loop and the functionally-critical TM domain [20; 36; 59]. Although the view that structure dictates protein function has been the holy grail of structural biology over the past century, the notion that structurally-disordered regions may also represent hot spots of protein function would have been perceived blasphemous even a decade ago. However, it is now rapidly becoming clear that structurally-disordered regions within proteins hold critical clues to their functional diversity and, in particular, their tight regulation [47–51].

In light of the aforementioned arguments, we undertook here detailed biophysical analysis of the full-length BclXL and investigated the role of the TM domain in dictating structure-function relationships within this important member of Bcl2 family. Our studies reveal for the first time that BclXL displays a high propensity to associate into higher-order oligomers

that are likely to be of physiological relevance. In particular, oligomerization of BclXL appears to be driven through domain-swapping such that the TM domain of one monomer occupies the canonical hydrophobic groove within the other monomer and vice versa in a trans-fashion. Over the past decade or so, homodimerization of proteins through domain-swapping has emerged as a common mechanism for protein oligomerization [60–65]. From a thermodynamic standpoint, such intermolecular association would allow two participating monomers to bury additional surface area culminating in not only enhanced stability but also providing a greater interacting molecular surface for further oligomerization (Figure 10a). We believe that such a mechanism also promotes the intermolecular association of BclXL homodimers into higher-order oligomers. Nonetheless, our in vitro and in silico analysis does not exclude the possibility that BclXL oligomerization may also ensue through an alternative inter-locking mechanism (Figure 10b), whereby the TM domain of one monomer locks onto the canonical hydrophobic groove of another monomer in a head-to-tail fashion in a manner akin to actin polymerization [66]. Regardless of the precise mechanism, BclXL oligomerization reported here appears to play a key role in fine-tuning its anti-apoptotic action by virtue of its ability to regulate ligand binding and membrane insertion. Consistent with this notion, truncation of TM domain completely abolishes oligomerization of BclXL and the resulting truncated construct exudes biophysical behavior distinct from the full-length protein including thermal stability, ligand binding and membrane insertion. Importantly, the ability of TM domain to trigger oligomerization of BclXL in solution appears to provide an allosteric switch for its auto-inhibition, activation and subsequent insertion into membranes. Thus, while ligand binding triggers the dissociation of BclXL oligomers into monomers, their subsequent insertion into membrane appears to be coupled to re-oligomerization into a functionally-active conformation.

On the basis of our data presented here, we propose a model to account for the self-association of BclXL into higher-order oligomers in concert with its hetero-association with repressors and activators and how such cross-talk is finely tuned in quiescent healthy cells versus apoptotic cells (Figure 10c). In quiescent non-apoptotic cells, BclXL either self-associates into higher-order oligomers and/or hetero-associates with effectors such as Bax and Bak, depending on the relative ratio of their cellular concentrations, to form repressor-effector complexes. In this manner, self-association into higher-order oligomers leads to inactivation of BclXL and hetero-association inactivates effectors. Upon receiving apoptotic stimuli, activators such as Bid and Bad compete with self-association of BclXL into higher-order oligomers and its hetero-association with effectors, leading to the formation of repressor-activator complexes as well as freeing up the effectors, which subsequently insert into MOM. This results in mitochondrial permeabilization leading to the release of apoptogenic factors that in turn induce cells to undergo apoptosis. Additionally, the displacement of the TM domain from the canonical hydrophobic groove within BclXL by BH3-only activators in a competitive manner triggers the translocation of BclXL into MOM via its TM domain (α9 helix) as well as the hairpin dagger (α5/α6 helices). Such solution-membrane transition would result in the disruption of the canonical hydrophobic groove allowing the BH3 ligands to drop off in agreement with the “hit-and-run” mechanism [29; 31–33]. Inside MOM, BclXL oligomer may exert its anti-apoptotic action by virtue of its ability to interfere with Bax and other effectors in the creation of mitochondrial pores so as to prevent the cytosolic release of apoptogenic factors and thereby halt the cell to undergo apoptosis. Notably, our model presented above is consistent with previous studies implicating the role of TM domain in mediating membrane insertion of apoptotic repressors [28; 32; 38], but contrasts other studies where regions other than the TM domain have been suggested [44; 67]. More importantly, consistent with our model is the observation that truncation of TM domain in both BclXL and Bcl2 repressors renders them cytosolic and impairs their ability to prevent apoptotic cell death [32; 68]. On the other hand, it has also been

shown that although BclW repressor associates with membranes in response to apoptotic stimuli, it neither promotes nor inhibits apoptosis [30].

Taken collectively, our study provides new mechanistic insights into the functional regulation of a key member of Bcl2 family and corroborates the notion that the TM domain promotes oligomerization of BclXL as previously reported by Zimmerberg and co-workers [69]. Importantly, this salient observation is further supported by studies conducted within live cells [32; 38]. However, our study also challenges the findings of other investigators. Notably, Hockenbery and co-workers recently demonstrated oligomerization of a truncated BclXL construct in which the TM domain is deleted [39], while Hill and coworkers reported lack of oligomerization in both the full-length BclXL and a truncated construct devoid of TM domain [43]. Although we are unable to account for the discrepancies observed between our data and those reported by others, we believe that these findings do not necessarily have to be mutually exclusive and the differences are likely to be explained by distinct experimental conditions employed in each study. We believe that the contradictory nature of our findings to those reported earlier will serve as a driving force for further advances in this field.

MATERIALS and METHODS

Sample preparation

BclXL_FL (residues 1–233) and BclXL_dTM (residues 1–200) constructs of human BclXL were cloned into pET30 bacterial expression vectors with an N-terminal His-tag using Novagen LIC technology (Figure 1a). The proteins were subsequently expressed in Escherichia coli BL21*(DE3) bacterial strain (Invitrogen) and purified on a Ni-NTA affinity column using standard procedures. Briefly, bacterial cells were grown at 20°C in Terrific Broth to an optical density of greater than unity at 600nm prior to induction with 0.5mM isopropyl β-D-1-thiogalactopyranoside (IPTG). The bacterial culture was further grown overnight at 20°C and the cells were subsequently harvested and disrupted using a BeadBeater (Biospec). After separation of cell debris at high-speed centrifugation, the cell lysate was loaded onto a Ni-NTA column and washed extensively with 20mM imidazole to remove non-specific binding of bacterial proteins to the column. The recombinant proteins were subsequently eluted with 200mM imidazole and dialyzed against an appropriate buffer to remove excess imidazole. Further treatment on a Hiload Superdex 200 size-exclusion chromatography (SEC) column coupled in-line with GE Akta FPLC system led to purification of BclXL_FL and BclXL_dTM constructs to an apparent homogeneity as judged by SDS-PAGE analysis. Final yield was typically between 10–20mg protein of apparent homogeneity per liter of bacterial culture. Protein concentration was determined by the fluorescence-based Quant-It assay (Invitrogen) and spectrophotometrically using extinction coefficients of 47,440 $M^{-1}cm^{-1}$ and 41,940 $M^{-1}cm^{-1}$ respectively calculated for the BclXL_FL and BclXL_dTM constructs using the online software ProtParam at ExPasy Server [70]. Results from both methods were in an excellent agreement. 20-mer peptides spanning various BH3 domains within human Bid, Bad and Bax proteins were commercially obtained from GenScript Corporation. The sequences of these peptides are shown in Figure 1b. The peptide concentrations were measured gravimetrically. Mixed DMPC/DHPC bicelles were prepared in an appropriate buffer at a final concentration of 30mM, at DMPC to DHPC molar ratio of 1:2, by stirring for 2h at 37°C.

Isothermal titration calorimetry

Isothermal titration calorimetry (ITC) experiments were performed on a Microcal VP-ITC instrument and data were acquired and processed using the integrated Microcal ORIGIN software. All measurements were repeated at least three times. Briefly, samples of

BclXL_FL and BclXL_dTM constructs and various BH3 peptides were prepared alone or in presence of DMPC/DHPC bicelles in 50mM Sodium phosphate, 100mM NaCl, 1mM EDTA and 5mM β-mercaptoethanol at pH 8.0. The experiments were initiated by injecting 25 × 10μl aliquots of 0.5–1mM of each BH3 peptide from the syringe into the calorimetric cell containing 1.8ml of 40–50 μM of BclXL_FL or BclXL_dTM construct at 25 °C. The change in thermal power as a function of each injection was automatically recorded using the ORIGIN software and the raw data were further processed to yield binding isotherms of heat release per injection as a function of molar ratio of each BH3 peptide to BclXL_FL or BclXL_dTM construct. The heats of mixing and dilution were subtracted from the heat of binding per injection by carrying out a control experiment in which the same buffer in the calorimetric cell was titrated against each peptide in an identical manner. To extract binding affinity (K_d) and binding enthalpy (ΔH), the ITC isotherms were iteratively fit to the following built-in function by non-linear least squares regression analysis using the integrated ORIGIN software:

$$q(i)=(n\Delta HVP/2)\{[1+(L/nP)+(K_d/nP)]-[[1+(L/nP)+(K_d/nP)]^2-(4L/nP)]^{1/2}\} \quad [1]$$

where q(i) is the heat release (kcal/mol) for the ith injection, n is the binding stoichiometry, V is the effective volume of protein solution in the calorimetric cell (1.46 ml), P is the total protein concentration in the calorimetric cell and L is the total concentration of peptide ligand added for the ith injection. Note that Eq [1] is derived from the binding of a ligand to a macromolecule using the law of mass action assuming a one-site model [71]. The free energy change (ΔG) upon ligand binding was calculated from the relationship:

$$\Delta G=RT\ln K_d \quad [2]$$

where R is the universal molar gas constant (1.99 cal/K/mol) and T is the absolute temperature. The entropic contribution (TΔS) to the free energy of binding was calculated from the relationship:

$$T\Delta S=\Delta H-\Delta G \quad [3]$$

where ΔH and ΔG are as defined above.

Differential scanning calorimetry

Differential scanning calorimetry (DSC) experiments were performed on a TA Nano-DSC instrument and data were acquired and processed using the integrated NanoAnalyze software. All measurements were repeated at least three times. Briefly, samples of BclXL_FL and BclXL_dTM constructs alone, in the presence of Bid_BH3 peptide and in the presence of DMPC/DHPC bicelles were prepared in 50mM Sodium phosphate at pH 8.0. All experiments were conducted on 10–50μM of each protein construct alone or at 10-molar excess of Bid_BH3 peptide in the 40–120°C temperature range at a heating rate (dT/dt) of 1°C/min under an excess pressure of 3atm. The change in thermal power (dQ/dt) as a function of temperature was automatically recorded using the NanoAnalyze software. Control experiments on the buffer alone, in the presence of Bid_BH3_peptide and in the presence of DMPC/DHPC bicelles were also conducted in an identical manner to generate baselines that were subtracted from the raw data to remove contribution due to the buffer and/or due to the peptide or bicelles. The raw data were further processed to yield the melting isotherms of excess heat capacity (C_p) as a function of temperature (T) using the following relationship:

$$C_p=[(dQ/dt)]/[(dT/dt)PV] \quad [4]$$

where P is the initial concentration of protein loaded into the calorimetric cell and V is the effective volume of calorimetric cell (0.3ml).

Analytical light scattering

Analytical light scattering (ALS) experiments were conducted on a Wyatt miniDAWN TREOS triple-angle static light scattering detector and Wyatt QELS dynamic light scattering detector coupled in-line with a Wyatt Optilab rEX differential refractive index detector and interfaced to a Hiload Superdex 200 size-exclusion chromatography column under the control of a GE Akta FPLC system within a chromatography refrigerator at 10°C. The BclXL_FL and BclXL_dTM constructs were prepared in 50mM Sodium phosphate, 100mM NaCl, 1mM EDTA and 5mM β-mercaptoethanol at pH 8.0 and loaded onto the column at a flow rate of 1ml/min and the data were automatically acquired using the ASTRA software. The starting concentrations of both protein constructs injected onto the column were between 10–50μM. The angular- and concentration-dependence of static light scattering (SLS) intensity of each protein construct resolved in the flow mode was measured by the Wyatt miniDAWN TREOS detector. The SLS data were analyzed according to the following built-in Zimm equation in ASTRA software [72; 73]:

$$[Kc/R_\theta]=((1/M)+2A_2c)[1+((16\pi^2(R_g)^2/3\lambda^2)\sin^2(\theta/2))] \quad [5]$$

where R_θ is the excess Raleigh ratio due to protein in the solution as a function of protein concentration c (mg/ml) and the scattering angle θ (42°, 90° and 138°), M is the observed molar mass of each protein species, A_2 is the second virial coefficient, λ is the wavelength of laser light in solution (658nm), R_g is the radius of gyration of protein, and K is given by the following relationship:

$$K=[4\pi^2n^2(dn/dc)^2]/N_A\lambda^4 \quad [6]$$

where n is the refractive index of the solvent, dn/dc is the refractive index increment of the protein in solution and N_A is the Avogadro's number ($6.02\times10^{23}mol^{-1}$). Under dilute protein concentrations ($c \rightarrow 0$), Eq [5] reduces to:

$$[Kc/R_\theta]=[1/M+((16\pi^2(R_g)^2/3M\lambda^2)\sin^2(\theta/2))] \quad [7]$$

Thus, a plot of $[Kc/R_\theta]$ versus $\sin^2(\theta/2)$ yields a straight line with slope $16\pi^2R_g^2/3M\lambda^2$ and y-intercept 1/M. Accordingly, M and R_g were respectively obtained in a global analysis from the y-intercept and the slope of linear fits of a range of $[Kc/R_\theta]-\sin^2(\theta/2)$ plots as a function of protein concentration along the elution profile of each protein species using SLS measurements at three scattering angles. It should however be noted that R_g was only determined for larger species that display angular-dependence of scattered light. Weighted-average molar mass (M_w) and number-average molar mass (M_n) were calculated from the following relationships:

$$M_w=\sum(c_iM_i)/\sum c_i \quad [8]$$

$$M_n = \sum c_i / \sum (c_i / M_i) \quad [9]$$

where c_i is the protein concentration and M_i is the observed molar mass at the ith slice within an elution profile. Likewise, R_g reported here represents the weighted-average value as defined by the following expression:

$$R_g = \sum (c_i R_{g,i}) / \sum c_i \quad [10]$$

where c_i is the protein concentration and $R_{g,i}$ is the observed radius of gyration at the ith slice within an elution profile. The time- and concentration-dependence of dynamic light scattering (DLS) intensity fluctuation of each protein construct resolved in the flow mode was measured by the Wyatt QELS detector positioned at 90° with respect to the incident laser beam. The DLS data were iteratively fit using non-linear least squares regression analysis to the following built-in equation in ASTRA software: software [74–76]:

$$G(\tau) = \alpha \mathrm{Exp}(-2\Gamma\tau) + \beta \quad [11]$$

where $G(\tau)$ is the autocorrelation function of dynamic light scattering intensity fluctuation I, τ is the delay time of autocorrelation function, Γ is the decay rate constant of autocorrelation function, α is the initial amplitude of autocorrelation function at zero delay time, and β is the baseline offset (the value of autocorrelation function at infinite delay time). Thus, fitting the above equation to a range of $G(\tau)$-τ plots as a function of protein concentration along the elution profile of each protein species computes the weighted-average value of Γ using DLS measurements at a scattering angle of 90°. Accordingly, the translational diffusion coefficient (D_t) of each protein species was calculated from the following relationship:

$$D_t = [(\Gamma\lambda^2)/(16\pi^2 n^2 \sin^2(\theta/2))] \quad [12]$$

where λ is the wavelength of laser light in solution (658nm), n is the refractive index of the solvent and θ is the scattering angle (90°). Additionally, the hydrodynamic radius (R_h) of each protein construct was determined from the Stokes-Einstein relationship:

$$R_h = [(k_B T)/(6\pi\eta D_t)] \quad [13]$$

where k_B is Boltzman's constant ($1.38\times10^{-23} JK^{-1}$), T is the absolute temperature and η is the solvent viscosity. Accordingly, the R_h reported here represents the weighted-average value as defined by the following expression:

$$R_h = \sum (c_i R_{h,i}) / \sum c_i \quad [14]$$

where c_i is the protein concentration and $R_{h,i}$ is the observed hydrodynamic radius at the ith slice within an elution profile. It should be noted that, in both the SLS and DLS measurements, protein concentration (c) along the elution profile of each protein species was automatically quantified in the ASTRA software from the change in refractive index (Δn) with respect to the solvent as measured by the Wyatt Optilab rEX detector using the following relationship:

$$c=(\Delta n)/(dn/dc) \quad [15]$$

where dn/dc is the refractive index increment of the protein in solution.

Steady-state fluorescence

Steady-state fluorescence (SSF) spectra were collected on a Jasco FP-6300 spectrofluorimeter using a quartz cuvette with a 10-mm pathlength at 25 °C. Briefly, experiments were conducted on 1–5μM of BclXL_FL or BclXL_dTM construct alone, in the presence of Bid_BH3 peptide (10-molar excess) and in the presence of DMPC/DHPC bicelles in 50mM Sodium phosphate, 100mM NaCl, 1mM EDTA and 5mM β-mercaptoethanol at pH 8.0. The excitation wavelength was 290nm and emission was acquired over the 300–500nm wavelength range. All data were recorded using a 2.5-nm bandwidth for both excitation and emission. Data were normalized against reference spectra to remove the contribution of buffer, Bid_BH3 peptide or DMPC/CHAPS bicelles.

Circular dichroism

Far-UV circular dichroism (CD) measurements were conducted on a Jasco J-815 spectrometer thermostatically controlled at 25°C. Experiments were conducted on 1–5μM of BclXL_FL or BclXL_dTM construct alone, in the presence of Bid_BH3 peptide (10-molar excess) and in the presence of DMPC/DHPC bicelles in 10mM Sodium phosphate at pH 8.0. Data were collected using a quartz cuvette with a 2-mm pathlength in the 190–250nm wavelength range. Data were normalized against reference spectra to remove the contribution of buffer, Bid_BH3 peptide or DMPC/CHAPS bicelles. Data were recorded with a slit bandwidth of 2nm at a scan rate of 10nm/min. Each data set represents an average of four scans acquired at 0.1nm intervals. Data were converted to molar ellipticity, [θ], as a function of wavelength (λ) of electromagnetic radiation using the equation:

$$[\theta]=[(10^5\Delta\varepsilon)/cl]\,\mathrm{deg.cm^2.dmol^{-1}} \quad [16]$$

where Δε is the observed ellipticity in mdeg, c is the peptide or protein concentration in μM and l is the cuvette pathlength in cm.

Transmission electron microscopy

Transmission electron microscopy (TEM) experiments were conducted on a Philips CM-10 electron microscope operating at a voltage of 80kV and images were photographed at a magnification of 105,000. Data were collected on a 25μM of BclXL_FL construct alone or in the presence of 10-molar excess of Bid_BH3 peptide in 50mM Sodium phosphate at pH 8.0 using negative staining. Briefly, formvar-coated copper grids (150-mesh) were floated on drops of each sample for 2 min. After briefly drying on a filter paper, the grids were immediately placed on drops of 2% phosphotungstic acid at pH 7.3 for 5 min. Excess liquid was wicked away with a filter paper and the grids were dried under vacuum desiccator for 3 days prior to imaging.

Molecular modeling

Molecular modeling (MM) was employed to build structural models of BclXL in various conformations using the MODELLER software based on homology modeling in combination with MOLMOL [77; 78]. Briefly, the structures modeled were those of BclXL monomers in which the TM domain is either exposed to solution (BclXL_solTM) or occupies the canonical hydrophobic groove (BclXL_cisTM) as well as the BclXL

homodimer in which the TM domain of one monomer occupies the canonical hydrophobic groove within the other monomer and vice versa in a domain-swapped trans-fashion (BclXL_transTM). In each case, solution structures of truncated BclXL in which the TM domain and the α1–α2 loop are missing (PDB# 1BXL), hereinafter referred to as tBclXL, and the full-length Bax in which the TM domain occupies the canonical hydrophobic groove (PDB# 1F16) were used as templates. More specifically, the entire models of BclXL in various conformations were built in homology with tBclXL (PDB# 1BXL) except for the TM domain, which was built in homology with the TM domain of Bax (PDB# 1F16), in a multiple-template alignment manner. Additionally, MOLMOL was used to bring various parts and/or monomers into optimal spatial orientations relative to each other in a rigid-body fashion. For the structural model of BclXL_solTM, the TM domain of Bax (PDB# 1F16) was dislodged away from the canonical hydrophobic groove so as to expose it to solution using MOLMOL prior to homology modeling in combination with tBclXL (PDB# 1BXL) in MODELLER. For the structural model of BclXL_cisTM, the TM domain of Bax (PDB# 1F16) was not physically perturbed from the canonical hydrophobic groove prior to homology modeling in combination with tBclXL (PDB# 1BXL) in MODELLER. In structural models of both BclXL_solTM and BclXL_cisTM, the residues within the α1–α2 loop were modeled without a template through energy minimization and molecular dynamics simulations. For the structural model of BclXL_transTM, pre-built structural models of two individual monomers of BclXL_cisTM were brought together in an optimal orientation in MOLMOL such that the α8–α9 loop within one monomer could be domain-swapped with TM domain of the other monomer without becoming taut. This requirement led to roughly parallel orientation of TM domains such that the sidechain moieties of apolar residues facing outward from the TM domain within one monomer were placed within van der Waals contact distance of sidechain moieties of apolar residues facing outward from the TM domain of the other monomer. Next, the α8–α9 loop preceding the TM domain within each BclXL_cisTM monomer was excised out and the resulting BclXL_cisTM monomers were used as a template to homology model the structure of BclXL_transTM. Notably, the residues within the α8–α9 loop within the BclXL_transTM structural model were modeled without a template through energy minimization and molecular dynamics simulations. For each structural model, a total of 100 atomic models were calculated and the structure with the lowest energy, as judged by the MODELLER Objective Function, was selected for further analysis. The atomic models were rendered using RIBBONS [79].

Molecular dynamics

Molecular dynamics (MD) simulations were performed with the GROMACS software [80; 81] using the integrated OPLS-AA force field [82; 83]. Briefly, the modeled structures of BclXL in various conformations (BclXL_solTM, BclXL_cisTM and BclXL_transTM) were centered within a cubic box and hydrated using the extended simple point charge (SPC/E) water model [84; 85]. The hydrated structures were energy-minimized with the steepest descent algorithm prior to equilibration under the NPT ensemble conditions, wherein the number of atoms (N), pressure (P) and temperature (T) within the system were respectively kept constant at ~50000, 1 bar and 300 K. The Particle-Mesh Ewald (PME) method was employed to compute long-range electrostatic interactions with a 10Å cut-off [86] and the Linear Constraint Solver (LINCS) algorithm to restrain bond lengths [87]. All MD simulations were performed under periodic boundary conditions (PBC) using the leap-frog integrator with a time step of 2fs. For the final MD production runs, data were collected every 10ps over a time scale of 100ns.

Acknowledgments

We are deeply indebted to Emre Dikici and Kendrick Turner from the Daunert Group for their generous help with CD data collection. This work was supported by the National Institutes of Health Grant R01-GM083897 and funds

from the USylvester Braman Family Breast Cancer Institute (to AF). CBM is a recipient of a postdoctoral fellowship from the National Institutes of Health (Award# T32-CA119929).

ABBREVIATIONS

ALS	Analytical light scattering
ANS	8-Anilinonaphthalene-1-sulfonate
Bad	Bcl2-associated death (promoter)
Bak	Bcl2 (homologous) antagonist/killer
Bax	Bcl2-associated X (protein)
Bcl2	B-cell lymphoma 2
BclXL	B-cell lymphoma extra large
BclXL_FL	Full-length BclXL (residues 1–233)
BclXL_dTM	BclXL in which the TM domain is deleted (residues 1–200)
BclXL_solTM	BclXL monomer in which the TM domain is exposed to solution
BclXL_cisTM	BclXL monomer in which the TM domain occupies the canonical hydrophobic groove
BclXL_transTM	BclXL homodimer in which the TM domain of one monomer occupies the canonical hydrophobic groove within the other monomer and vice versa in a domain-swapped trans-fashion
BH1	Bcl2 homology 1 (domain)
BH2	Bcl2 homology 2 (domain)
BH3	Bcl2 homology 3 (domain)
BH4	Bcl2 homology 4 (domain)
Bid	BH3-interacting domain (death agonist)
CD	Circular dichroism
DHPC	1,2-Dihexanoyl-sn-glycero-3-phosphocholine
DLS	Dynamic light scattering
DMPC	1,2-Dimyristoyl-sn-glycero-3-phosphocholine
DSC	Differential scanning calorimetry
MOM	mitochondrial outer membrane
TEM	Transmission electron microscopy
ITC	Isothermal titration calorimetry
LIC	Ligation-independent cloning
MD	Molecular dynamics
MM	Molecular modeling
SEC	Size-exclusion chromatography
SLS	Static light scattering
SSF	Steady-state fluorescence

References

1. Thompson CB. Apoptosis in the pathogenesis and treatment of disease. Science. 1995; 267:1456–62. [PubMed: 7878464]
2. Reed JC. Mechanisms of apoptosis. Am J Pathol. 2000; 157:1415–30. [PubMed: 11073801]
3. Yip KW, Reed JC. Bcl-2 family proteins and cancer. Oncogene. 2008; 27:6398–406. [PubMed: 18955968]
4. Youle RJ, Strasser A. The BCL-2 protein family: opposing activities that mediate cell death. Nat Rev Mol Cell Biol. 2008; 9:47–59. [PubMed: 18097445]
5. Kuwana T, Newmeyer DD. Bcl-2-family proteins and the role of mitochondria in apoptosis. Curr Opin Cell Biol. 2003; 15:691–9. [PubMed: 14644193]
6. Adams JM, Cory S. The Bcl-2 protein family: arbiters of cell survival. Science. 1998; 281:1322–6. [PubMed: 9735050]
7. Gross A, McDonnell JM, Korsmeyer SJ. BCL-2 family members and the mitochondria in apoptosis. Genes Dev. 1999; 13:1899–911. [PubMed: 10444588]
8. Korsmeyer SJ. BCL-2 gene family and the regulation of programmed cell death. Cancer Res. 1999; 59:1693s–1700s. [PubMed: 10197582]
9. Chipuk JE, Moldoveanu T, Llambi F, Parsons MJ, Green DR. The BCL-2 family reunion. Mol Cell. 2010; 37:299–310. [PubMed: 20159550]
10. Dejean LM, Ryu SY, Martinez-Caballero S, Teijido O, Peixoto PM, Kinnally KW. MAC and Bcl-2 family proteins conspire in a deadly plot. Biochim Biophys Acta. 2010; 1797:1231–8. [PubMed: 20083086]
11. Dewson G, Kluck RM. Mechanisms by which Bak and Bax permeabilise mitochondria during apoptosis. J Cell Sci. 2009; 122:2801–8. [PubMed: 19795525]
12. Chipuk JE, Fisher JC, Dillon CP, Kriwacki RW, Kuwana T, Green DR. Mechanism of apoptosis induction by inhibition of the anti-apoptotic BCL-2 proteins. Proc Natl Acad Sci U S A. 2008; 105:20327–32. [PubMed: 19074266]
13. Chipuk JE, Green DR. How do BCL-2 proteins induce mitochondrial outer membrane permeabilization? Trends Cell Biol. 2008; 18:157–64. [PubMed: 18314333]
14. Lakey JH, van der Goot FG, Pattus F. All in the family: the toxic activity of pore-forming colicins. Toxicology. 1994; 87:85–108. [PubMed: 8160190]
15. London E. Diphtheria toxin: membrane interaction and membrane translocation. Biochim Biophys Acta. 1992; 1113:25–51. [PubMed: 1550860]
16. Zakharov SD, Cramer WA. Colicin crystal structures: pathways and mechanisms for colicin insertion into membranes. Biochim Biophys Acta. 2002; 1565:333–46. [PubMed: 12409205]
17. van der Goot FG, Gonzalez-Manas JM, Lakey JH, Pattus F. A ‘molten-globule’ membrane-insertion intermediate of the pore-forming domain of colicin A. Nature. 1991; 354:408–10. [PubMed: 1956406]
18. Schendel SL, Montal M, Reed JC. Bcl-2 family proteins as ion-channels. Cell Death Differ. 1998; 5:372–80. [PubMed: 10200486]
19. Shimizu S, Narita M, Tsujimoto Y. Bcl-2 family proteins regulate the release of apoptogenic cytochrome c by the mitochondrial channel VDAC. Nature. 1999; 399:483–7. [PubMed: 10365962]
20. Petros AM, Olejniczak ET, Fesik SW. Structural biology of the Bcl-2 family of proteins. Biochim Biophys Acta. 2004; 1644:83–94. [PubMed: 14996493]
21. Krajewski S, Tanaka S, Takayama S, Schibler MJ, Fenton W, Reed JC. Investigation of the subcellular distribution of the bcl-2 oncoprotein: residence in the nuclear envelope, endoplasmic reticulum, and outer mitochondrial membranes. Cancer Res. 1993; 53:4701–14. [PubMed: 8402648]
22. Gonzalez-Garcia M, Perez-Ballestero R, Ding L, Duan L, Boise LH, Thompson CB, Nunez G. bcl-XL is the major bcl-x mRNA form expressed during murine development and its product localizes to mitochondria. Development. 1994; 120:3033–42. [PubMed: 7607090]

23. Zha H, Fisk HA, Yaffe MP, Mahajan N, Herman B, Reed JC. Structure-function comparisons of the proapoptotic protein Bax in yeast and mammalian cells. Mol Cell Biol. 1996; 16:6494–508. [PubMed: 8887678]
24. Gavathiotis E, Suzuki M, Davis ML, Pitter K, Bird GH, Katz SG, Tu HC, Kim H, Cheng EH, Tjandra N, Walensky LD. BAX activation is initiated at a novel interaction site. Nature. 2008; 455:1076–81. [PubMed: 18948948]
25. Walensky LD, Pitter K, Morash J, Oh KJ, Barbuto S, Fisher J, Smith E, Verdine GL, Korsmeyer SJ. A stapled BID BH3 helix directly binds and activates BAX. Mol Cell. 2006; 24:199–210. [PubMed: 17052454]
26. Dai H, Smith A, Meng XW, Schneider PA, Pang YP, Kaufmann SH. Transient binding of an activator BH3 domain to the Bak BH3-binding groove initiates Bak oligomerization. J Cell Biol. 2011; 194:39–48. [PubMed: 21727192]
27. Suzuki M, Youle RJ, Tjandra N. Structure of Bax: coregulation of dimer formation and intracellular localization. Cell. 2000; 103:645–54. [PubMed: 11106734]
28. Hinds MG, Lackmann M, Skea GL, Harrison PJ, Huang DC, Day CL. The structure of Bcl-w reveals a role for the C-terminal residues in modulating biological activity. EMBO J. 2003; 22:1497–507. [PubMed: 12660157]
29. Denisov AY, Madiraju MS, Chen G, Khadir A, Beauparlant P, Attardo G, Shore GC, Gehring K. Solution structure of human BCL-w: modulation of ligand binding by the C-terminal helix. J Biol Chem. 2003; 278:21124–8. [PubMed: 12651847]
30. Wilson-Annan J, O'Reilly LA, Crawford SA, Hausmann G, Beaumont JG, Parma LP, Chen L, Lackmann M, Lithgow T, Hinds MG, Day CL, Adams JM, Huang DC. Proapoptotic BH3-only proteins trigger membrane integration of prosurvival Bcl-w and neutralize its activity. J Cell Biol. 2003; 162:877–87. [PubMed: 12952938]
31. Kim PK, Annis MG, Dlugosz PJ, Leber B, Andrews DW. During apoptosis bcl-2 changes membrane topology at both the endoplasmic reticulum and mitochondria. Mol Cell. 2004; 14:523–9. [PubMed: 15149601]
32. Jeong SY, Gaume B, Lee YJ, Hsu YT, Ryu SW, Yoon SH, Youle RJ. Bcl-x(L) sequesters its C-terminal membrane anchor in soluble, cytosolic homodimers. EMBO J. 2004; 23:2146–55. [PubMed: 15131699]
33. Denisov AY, Chen G, Sprules T, Moldoveanu T, Beauparlant P, Gehring K. Structural model of the BCL-w-BID peptide complex and its interactions with phospholipid micelles. Biochemistry. 2006; 45:2250–6. [PubMed: 16475813]
34. Kelekar A, Chang BS, Harlan JE, Fesik SW, Thompson CB. Bad is a BH3 domain-containing protein that forms an inactivating dimer with Bcl-XL. Mol Cell Biol. 1997; 17:7040–6. [PubMed: 9372935]
35. Petros AM, Nettesheim DG, Wang Y, Olejniczak ET, Meadows RP, Mack J, Swift K, Matayoshi ED, Zhang H, Thompson CB, Fesik SW. Rationale for Bcl-xL/Bad peptide complex formation from structure, mutagenesis, and biophysical studies. Protein Sci. 2000; 9:2528–34. [PubMed: 11206074]
36. Petros AM, Medek A, Nettesheim DG, Kim DH, Yoon HS, Swift K, Matayoshi ED, Oltersdorf T, Fesik SW. Solution structure of the antiapoptotic protein bcl-2. Proc Natl Acad Sci U S A. 2001; 98:3012–7. [PubMed: 11248023]
37. Li H, Hayashi F, Koshiba S, Inoue M, Kigawa T, Yokoyama S. Solution Structure of the C-terminal Phosphotyrosine Interaction Domain of APBB2 from Mouse. To be published; PDB code: 1WGU. 2004
38. Ospina A, Lagunas-Martinez A, Pardo J, Carrodeguas JA. Protein oligomerization mediated by the transmembrane carboxyl terminal domain of Bcl-XL. FEBS Lett. 2011; 585:2935–42. [PubMed: 21856303]
39. O'Neill JW, Manion MK, Maguire B, Hockenbery DM. BCL-XL dimerization by three-dimensional domain swapping. J Mol Biol. 2006; 356:367–81. [PubMed: 16368107]
40. Denisov AY, Sprules T, Fraser J, Kozlov G, Gehring K. Heat-induced dimerization of BCL-xL through alpha-helix swapping. Biochemistry. 2007; 46:734–40. [PubMed: 17223694]

41. Lee EF, Dewson G, Smith BJ, Evangelista M, Pettikiriarachchi A, Dogovski C, Perugini MA, Colman PM, Fairlie WD. Crystal structure of a BCL-W domain-swapped dimer: implications for the function of BCL-2 family proteins. Structure. 2011; 19:1467–76. [PubMed: 22000515]
42. Losonczi JA, Olejniczak ET, Betz SF, Harlan JE, Mack J, Fesik SW. NMR studies of the anti-apoptotic protein Bcl-xL in micelles. Biochemistry. 2000; 39:11024–33. [PubMed: 10998239]
43. Thuduppathy GR, Craig JW, Kholodenko V, Schon A, Hill RB. Evidence that membrane insertion of the cytosolic domain of Bcl-xL is governed by an electrostatic mechanism. J Mol Biol. 2006; 359:1045–58. [PubMed: 16650855]
44. Thuduppathy GR, Terrones O, Craig JW, Basanez G, Hill RB. The N-terminal domain of Bcl-xL reversibly binds membranes in a pH-dependent manner. Biochemistry. 2006; 45:14533–42. [PubMed: 17128992]
45. Kaufmann T, Schlipf S, Sanz J, Neubert K, Stein R, Borner C. Characterization of the signal that directs Bcl-x(L), but not Bcl-2, to the mitochondrial outer membrane. J Cell Biol. 2003; 160:53–64. [PubMed: 12515824]
46. Sattler M, Liang H, Nettesheim D, Meadows RP, Harlan JE, Eberstadt M, Yoon HS, Shuker SB, Chang BS, Minn AJ, Thompson CB, Fesik SW. Structure of Bcl-xL-Bak peptide complex: recognition between regulators of apoptosis. Science. 1997; 275:983–6. [PubMed: 9020082]
47. Dunker AK, Lawson JD, Brown CJ, Williams RM, Romero P, Oh JS, Oldfield CJ, Campen AM, Ratliff CM, Hipps KW. Intrinsically Disordered Protein. J Mol Graph Model. 2001; 19:26–59. [PubMed: 11381529]
48. Dunker AK, Cortese MS, Romero P, Iakoucheva LM, Uversky VN. Flexible nets. The roles of intrinsic disorder in protein interaction networks. FEBS J. 2005; 272:5129–48. [PubMed: 16218947]
49. Liu J, Perumal NB, Oldfield CJ, Su EW, Uversky VN, Dunker AK. Intrinsic disorder in transcription factors. Biochemistry. 2006; 45:6873–88. [PubMed: 16734424]
50. Haynes C, Oldfield CJ, Ji F, Klitgord N, Cusick ME, Radivojac P, Uversky VN, Vidal M, Iakoucheva LM. Intrinsic disorder is a common feature of hub proteins from four eukaryotic interactomes. PLoS Comput Biol. 2006; 2:e100. [PubMed: 16884331]
51. Uversky VN. Intrinsically disordered proteins from A to Z. Int J Biochem Cell Biol. 2011; 43:1090–103. [PubMed: 21501695]
52. Mason JM, Arndt KM. Coiled coil domains: stability, specificity, and biological implications. Chembiochem. 2004; 5:170–6. [PubMed: 14760737]
53. Chang BS, Minn AJ, Muchmore SW, Fesik SW, Thompson CB. Identification of a novel regulatory domain in Bcl-X(L) and Bcl-2. EMBO J. 1997; 16:968–77. [PubMed: 9118958]
54. Tsujimoto Y, Cossman J, Jaffe E, Croce CM. Involvement of the bcl-2 gene in human follicular lymphoma. Science. 1985; 228:1440–3. [PubMed: 3874430]
55. Tsujimoto Y, Croce CM. Analysis of the structure, transcripts, and protein products of bcl-2, the gene involved in human follicular lymphoma. Proc Natl Acad Sci U S A. 1986; 83:5214–8. [PubMed: 3523487]
56. Haldar S, Reed JC, Beatty C, Croce CM. Role of bcl-2 in growth factor triggered signal transduction. Cancer Res. 1990; 50:7399–401. [PubMed: 2121338]
57. Korsmeyer SJ, McDonnell TJ, Nunez G, Hockenbery D, Young R. Bcl-2: B cell life, death and neoplasia. Curr Top Microbiol Immunol. 1990; 166:203–7. [PubMed: 2073800]
58. Hockenbery D, Nunez G, Milliman C, Schreiber RD, Korsmeyer SJ. Bcl-2 is an inner mitochondrial membrane protein that blocks programmed cell death. Nature. 1990; 348:334–6. [PubMed: 2250705]
59. Muchmore SW, Sattler M, Liang H, Meadows RP, Harlan JE, Yoon HS, Nettesheim D, Chang BS, Thompson CB, Wong SL, Ng SL, Fesik SW. X-ray and NMR structure of human Bcl-xL, an inhibitor of programmed cell death. Nature. 1996; 381:335–41. [PubMed: 8692274]
60. Bennett MJ, Choe S, Eisenberg D. Domain swapping: entangling alliances between proteins. Proc Natl Acad Sci U S A. 1994; 91:3127–31. [PubMed: 8159715]
61. Liu Y, Eisenberg D. 3D domain swapping: as domains continue to swap. Protein Sci. 2002; 11:1285–99. [PubMed: 12021428]

62. Liu Y, Gotte G, Libonati M, Eisenberg D. Structures of the two 3D domain-swapped RNase A trimers. Protein Sci. 2002; 11:371–80. [PubMed: 11790847]
63. Janowski R, Kozak M, Jankowska E, Grzonka Z, Grubb A, Abrahamson M, Jaskolski M. Human cystatin C, an amyloidogenic protein, dimerizes through three-dimensional domain swapping. Nat Struct Biol. 2001; 8:316–20. [PubMed: 11276250]
64. Bennett MJ, Sawaya MR, Eisenberg D. Deposition diseases and 3D domain swapping. Structure. 2006; 14:811–24. [PubMed: 16698543]
65. Benfield AP, Whiddon BB, Clements JH, Martin SF. Structural and energetic aspects of Grb2-SH2 domain-swapping. Arch Biochem Biophys. 2007; 462:47–53. [PubMed: 17466257]
66. Dominguez R, Holmes KC. Actin structure and function. Annu Rev Biophys. 2011; 40:169–86. [PubMed: 21314430]
67. Franzin CM, Choi J, Zhai D, Reed JC, Marassi FM. Structural studies of apoptosis and ion transport regulatory proteins in membranes. Magn Reson Chem. 2004; 42:172–9. [PubMed: 14745797]
68. Nguyen M, Branton PE, Walton PA, Oltvai ZN, Korsmeyer SJ, Shore GC. Role of membrane anchor domain of Bcl-2 in suppression of apoptosis caused by E1B-defective adenovirus. J Biol Chem. 1994; 269:16521–4. [PubMed: 8206964]
69. Basanez G, Zhang J, Chau BN, Maksaev GI, Frolov VA, Brandt TA, Burch J, Hardwick JM, Zimmerberg J. Pro-apoptotic cleavage products of Bcl-xL form cytochrome c-conducting pores in pure lipid membranes. J Biol Chem. 2001; 276:31083–91. [PubMed: 11399768]
70. Gasteiger, E.; Hoogland, C.; Gattiker, A.; Duvaud, S.; Wilkins, MR.; Appel, RD.; Bairoch, A. Protein Identification and Analysis Tools on the ExPASy Server. In: Walker, JM., editor. The Proteomics Protocols Handbook. Humana Press; Totowa, New Jersey, USA: 2005. p. 571-607.
71. Wiseman T, Williston S, Brandts JF, Lin LN. Rapid measurement of binding constants and heats of binding using a new titration calorimeter. Anal Biochem. 1989; 179:131–137. [PubMed: 2757186]
72. Zimm BH. The Scattering of Light and the Radial Distribution Function of High Polymer Solutions. J Chem Phys. 1948; 16:1093–1099.
73. Wyatt PJ. Light Scattering and the Absolute Characterization of Macromolecules. Anal Chim Acta. 1993; 272:1–40.
74. Berne, BJ.; Pecora, R. Dynamic Light Scattering. Wiley; New York: 1976.
75. Chu, B. Laser Light Scattering: Basic Principles and Practice. Academic; Boston: 1991.
76. Koppel DE. Analysis of Macromolecular Polydispersity in Intensity Correlation Spectroscopy. J Chem Phys. 1972; 57:4814–4820.
77. Marti-Renom MA, Stuart AC, Fiser A, Sanchez R, Melo F, Sali A. Comparative Protein Structure Modeling of Genes and Genomes. Annu Rev Biophys Biomol Struct. 2000; 29:291–325. [PubMed: 10940251]
78. Koradi R, Billeter M, Wuthrich K. MOLMOL: a program for display and analysis of macromolecular structures. J Mol Graph. 1996; 14:51–55. [PubMed: 8744573]
79. Carson M. Ribbons 2.0. J Appl Crystallogr. 1991; 24:958–961.
80. Van Der Spoel D, Lindahl E, Hess B, Groenhof G, Mark AE, Berendsen HJ. GROMACS: fast, flexible, and free. J Comput Chem. 2005; 26:1701–18. [PubMed: 16211538]
81. Hess B. GROMACS 4: Algorithms for Highly Efficient, Load-Balanced, and Scalable Molecular Simulation. J Chem Theory Comput. 2008; 4:435–447.
82. Jorgensen WL, Tirado-Rives J. The OPLS Force Field for Proteins: Energy Minimizations for Crystals of Cyclic Peptides and Crambin. J Am Chem Soc. 1988; 110:1657–1666.
83. Kaminski GA, Friesner RA, Tirado-Rives J, Jorgensen WL. Evaluation and Reparametrization of the OPLS-AA Force Field for Proteins via Comparison with Accurate Quantum Chemical Calculations on Peptides. J Phys Chem B. 2001; 105:6474–6487.
84. Toukan K, Rahman A. Molecular-dynamics study of atomic motions in water. Physical Review B. 1985; 31:2643–2648.
85. Berendsen HJC, Grigera JR, Straatsma TP. The Missing Term in Effective Pair Potentials. J Phys Chem. 1987; 91:6269–6271.

86. Darden TA, York D, Pedersen L. Particle mesh Ewald: An N.log(N) method for Ewald sums in large systems. J Chem Phys. 1993; 98:10089–10092.

87. Hess B, Bekker H, Berendsen HJC, Fraaije JGEM. LINCS: A linear constraint solver for molecular simulations. J Comput Chem. 1997; 18:1463–1472.

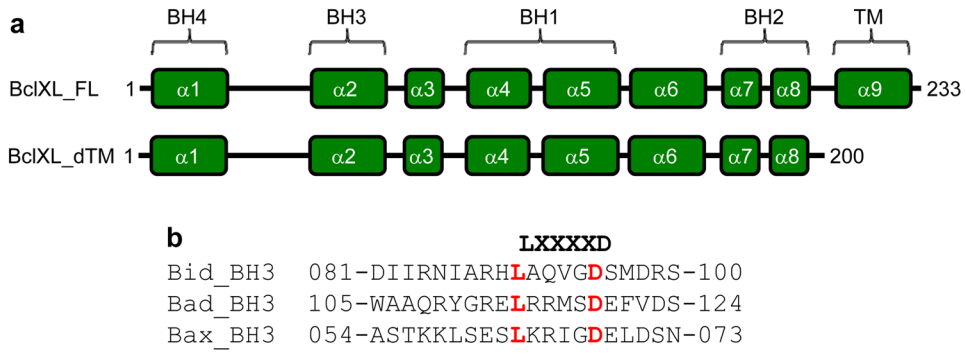

Figure 1.

BclXL domain organization and BH3 ligands. (a) Human BclXL is comprised of the BH4-BH3-BH1-BH2-TM modular organization, with a C-terminal transmembrane (TM) domain preceded by four N-terminal Bcl2 homology (BH) domains. The relationship between the various helices (α1–α9) punctuating the topological fold of BclXL and the BH domains is clearly indicated for clarity. While the BclXL_FL construct represents the full-length protein with the above modular organization, the C-terminal TM domain has been deleted in BclXL_dTM construct in order to investigate its function in the biological function of BclXL in this study. The numerals indicate amino acid boundaries within corresponding protein sequences. (b) Amino acid sequence alignment of 20-mer peptides spanning various BH3 domains within human Bid, Bad and Bax proteins. The numerals indicate amino acid boundaries within corresponding protein sequences. The LXXXXD motif characteristic of all BH3 domains is highlighted.

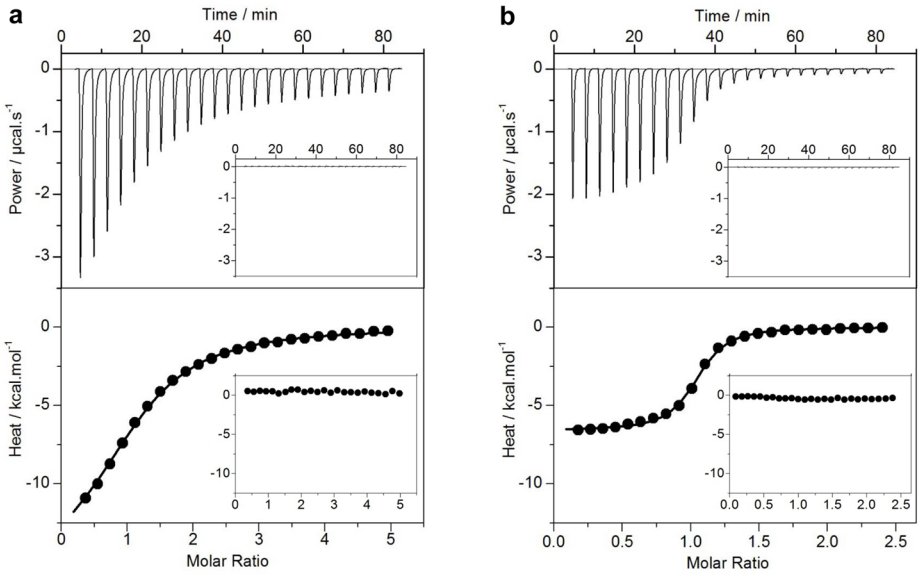

Figure 2.

ITC analysis for the binding of Bid_BH3 peptide to BclXL_FL (a) and BclXL_dTM (b) constructs. The upper panels show raw ITC data expressed as change in thermal power with respect to time over the period of titration. In the lower panels, change in molar heat is expressed as a function of molar ratio of Bid_BH3 peptide to the corresponding construct. The solid lines in the lower panels show the fit of data to a one-site model, as embodied in Eq [1], using the ORIGIN software. The insets show same titrations conducted in the presence of DMPC/DHPC bicelles.

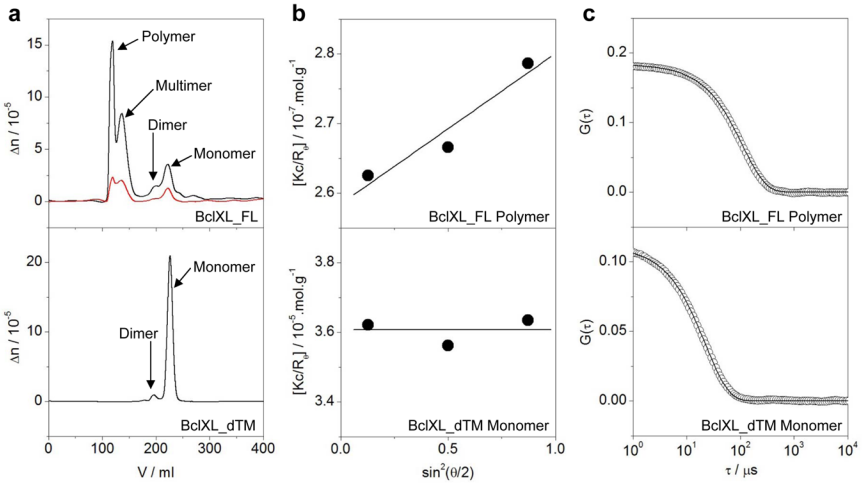

Figure 3.

ALS analysis for BclXL_dTM and BclXL_FL constructs as indicated. (a) Elution profiles as monitored by the differential refractive index (Δn) plotted as a function of elution volume (V) for BclXL_FL (top panel) and BclXL_dTM (bottom panel) constructs. Note that the elution profile for BclXL_FL construct is shown at both 50μM (black) and 10μM (red) initial protein concentrations loaded onto the Superdex-200 column, while that for BclXL_dTM construct is only shown at 50μM (black). (b) Partial Zimm plots obtained from analytical SLS measurements at a specific protein concentration for BclXL_FL polymer (top panel) and BclXL_dTM monomer (bottom panel). The solid lines through the data points represent linear fits. (c) Autocorrelation function plots obtained from analytical DLS measurements at a specific protein concentration for BclXL_FL polymer (top panel) and BclXL_dTM monomer (bottom panel). The solid lines through the data points represent non-linear least squares fits to Eq [11].

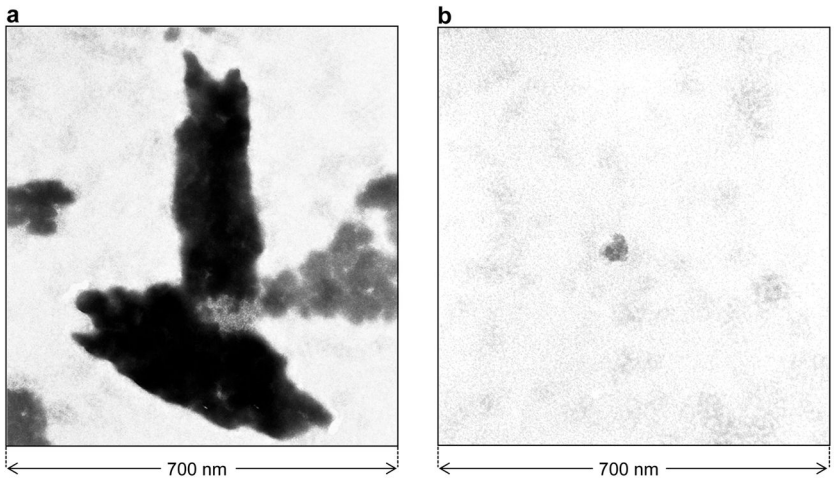

Figure 4.
TEM micrographs of negatively-stained BclXL_FL construct alone (a) and in the presence of Bid_BH3 peptide (b).

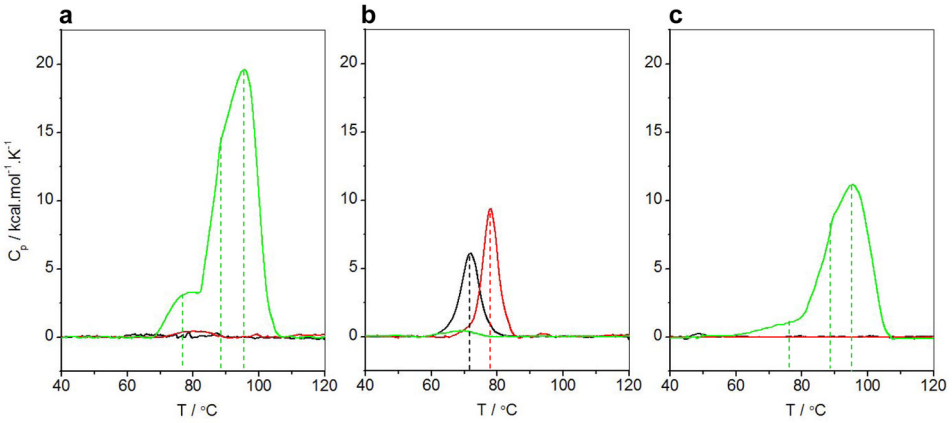

Figure 5.

DSC isotherms for BclXL_FL construct at 50μM (a), BclXL_dTM construct at 50μM (b) and BclXL_FL construct at 10μM (c) alone (black), in the presence of excess Bid_BH3 peptide (red) and in the presence of excess DMPC/DHPC bicelles (green). The dashed vertical lines indicate T_m values of various thermal phases.

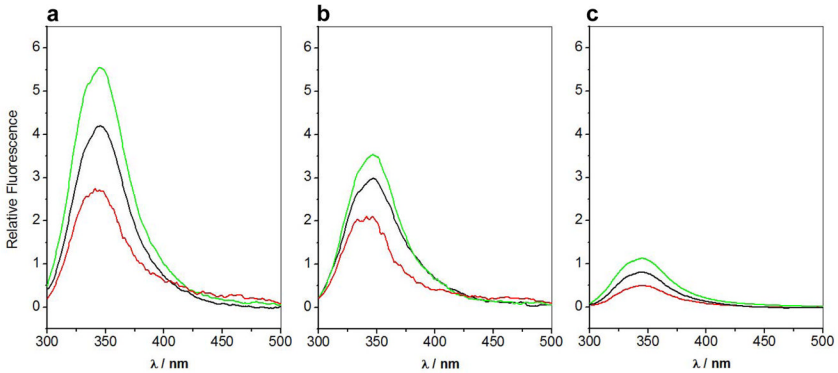

Figure 6.

SSF spectra of BclXL_FL construct at 5μM (a), BclXL_dTM construct at 5μM (b) and SEC-resolved fractions containing higher-order oligomers of BclXL_FL at 1μM (c) alone (black), in the presence of excess Bid_BH3 peptide (red) and in the presence of excess DMPC/DHPC bicelles (green).

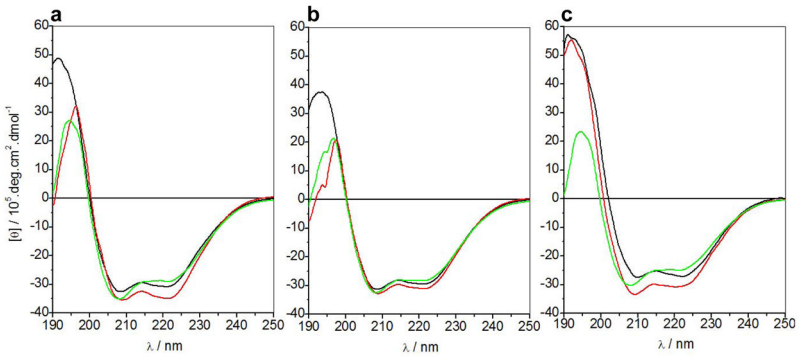

Figure 7.

Far-UV CD spectra of BclXL_FL construct at 5μM (a), BclXL_dTM construct at 5μM (b) and SEC-resolved fractions containing higher-order oligomers of BclXL_FL at 1μM (c) alone (black), in the presence of excess Bid_BH3 peptide (red) and in the presence of excess DMPC/DHPC bicelles (green).

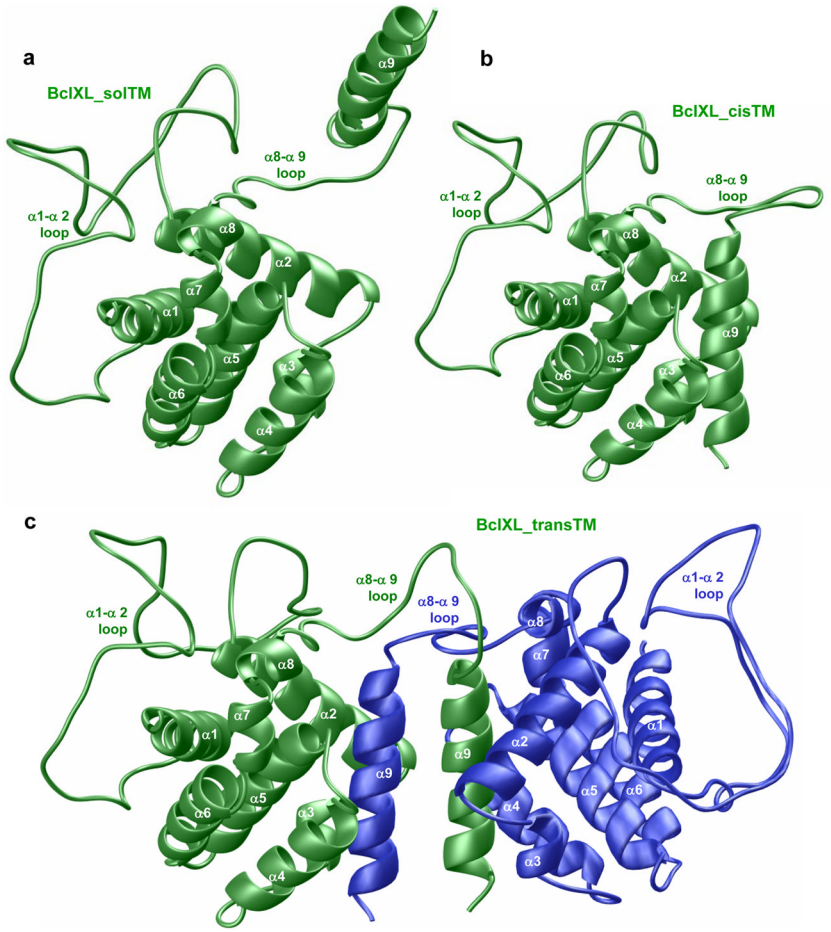

Figure 8.

Structural models of full-length BclXL in three distinct conformations with respect to the C-terminal TM domain (α9 helix). (a) Monomeric BclXL with the TM domain exposed to solution (BclXL_solTM). (b) Monomeric BclXL with the TM domain bound to the canonical hydrophobic groove (BclXL_cisTM). (c) Homodimeric BclXL with the TM domain bound to the canonical hydrophobic groove but swapped in an intermolecular trans-fashion — the TM domain of one monomer (green) is bound to the other monomer (blue) and vice versa (BclXL_transTM).

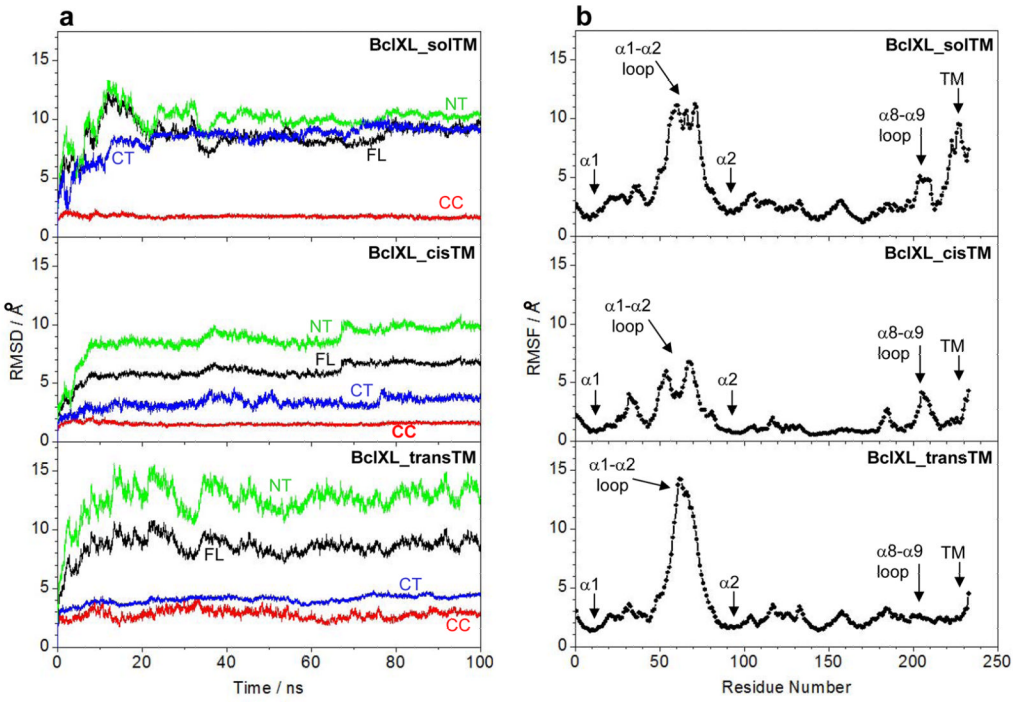

Figure 9.

MD analysis on structural models of full-length BclXL in three distinct conformations with respect to the C-terminal TM domain (α9 helix). (a) Root mean square deviation (RMSD) of backbone atoms (N, Cα and C) for residues 1–233 (black), residues 86–195 (red), residues 1–85 (green) and residues 196–233 (blue) within each simulated structure relative to the initial modeled structure of BclXL_solTM, BclXL_cisTM and BclXL_transTM as a function of simulation time. Note that, for each construct, the RMSD of full-length (FL) protein spanning residues 1–233 is also deconvoluted into the central core (CC) region spanning residues 86–195, the N-terminal (NT) region spanning residues 1–85, and the C-terminal (CT) region spanning residues 196–233. (b) Root mean square fluctuation (RMSF) of backbone atoms (N, Cα and C) averaged over the entire course of corresponding MD trajectory of BclXL_solTM, BclXL_cisTM and BclXL_transTM as a function of residue number.

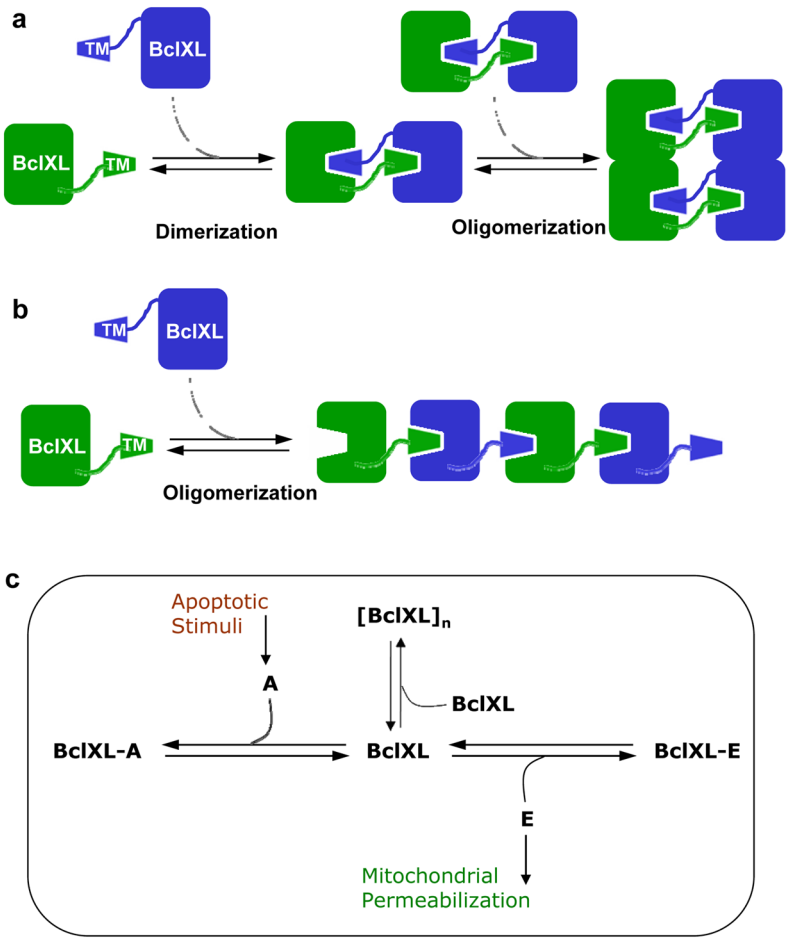

Figure 10.

Models for BclXL oligomerization and its role in apoptotic regulation. (a) Oligomerization of BclXL via a domain-swapped mechanism. The TM domain of one monomer (green) occupies the canonical hydrophobic groove within another monomer (blue) and vice versa to form a homodimer. The resulting homodimers, due to greater interacting molecular surface area, further self-associate into higher-order oligomers. (b) Oligomerization of BclXL via an inter-locking mechanism. The TM domain of one monomer (green) occupies the canonical hydrophobic groove within another monomer (blue) in a head-to-tail fashion so as to aid the assembly of much larger oligomers. (c) A thermodynamic cycle depicting how various linked-equilibria determine the fate of BclXL repressor to self-associate into higher-order $[BclXL]_n$ oligomers versus hetero-association with activator (A) and effector (E) molecules in quiescent versus apoptotic cells. In quiescent non-apoptotic cells, BclXL either self-associates into higher-order $[BclXL]_n$ oligomers and/or hetero-associates with effectors such as Bax and Bak, depending on the relative ratio of their cellular concentrations, to form BclXL-E repressor-effector complexes. In this manner, self-association into higher-order oligomers leads to inactivation of BclXL and hetero-association inactivates effectors. Upon receiving apoptotic stimuli, activators such as Bid and Bad compete with self-association of BclXL into higher-order oligomers and its hetero-association with effectors, leading to the formation of BclXL-A repressor-activator complexes as well as freeing up the effectors, which subsequently insert into MOM. This results in mitochondrial permeabilization leading to the release of apoptogenic factors that in turn induce cells to undergo apoptosis.

Table 1

Thermodynamic parameters for the binding of various BH3 peptides to BclXL_FL and BclXL_dTM constructs

	BclXL_FL				BclXL_dTM			
Peptide	**K_d/μM**	**ΔH/kcal.mol^{-1}**	**TΔS/kcal.mol^{-1}**	**ΔG/kcal.mol^{-1}**	**K_d/μM**	**ΔH/kcal.mol^{-1}**	**TΔS/kcal.mol^{-1}**	**ΔG/kcal.mol^{-1}**
Bid_BH3	9.97 ± 1.25	−18.74 ± 0.19	−11.91 ± 0.17	−6.82 ± 0.01	0.79 ± 0.08	−6.45 ± 0.07	+1.88 ± 0.03	−8.32 ± 0.04
Bad_BH3	10.30 ± 1.42	−14.19 ± 0.08	−7.37 ± 0.04	−6.81 ± 0.04	0.89 ± 0.12	−7.84 ± 0.14	+0.46 ± 0.11	−8.26 ± 0.02
Bax_BH3	35.10 ± 3.72	−19.40 ± 0.30	−13.31 ± 0.25	−6.08 ± 0.06	3.25 ± 0.27	−5.55 ± 0.07	+1.94 ± 0.08	−7.50 ± 0.01

All parameters were obtained from ITC measurements at pH 8.0 and 25°C. All binding stoichiometries were 1:1 and generally agreed to within ±10%. Errors were calculated from at least three independent measurements. All errors are given to one standard deviation.

Table 2

Comparison of hydrodynamic parameters for BCLXL_dTM and BclXL_FL constructs

Construct	Associativity	M_w/kD	M_n/kD	M_w/M_n	R_g/Å	R_h/Å	R_g/R_h
BclXL_dTM	Monomer	28 ± 2	28 ± 2	1.00 ± 0.00	ND	33 ± 2	ND
	Dimer	54 ± 2	54 ± 2	1.00 ± 0.01	ND	41 ± 3	ND
BclXL_FL	Monomer	31 ± 1	31 ± 1	1.00 ± 0.01	ND	36 ± 1	ND
	Dimer	62 ± 3	61 ± 3	1.01 ± 0.01	ND	47 ± 2	ND
	Multimer	361 ± 26	321 ± 25	1.14 ± 0.02	107 ± 4	99 ± 2	1.10 ± 0.01
	Polymer	3355 ± 188	3134 ± 147	1.17 ± 0.02	198 ± 8	175 ± 6	1.13 ± 0.02

All parameters were obtained from ALS measurements at pH 8 and 10°C. Note that the calculated molar masses of recombinant BclXL_dTM and BclXL_FL constructs from their respective amino acid sequences are 27kD and 31kD, respectively. Errors were calculated from at least three independent measurements. All errors are given to one standard deviation. Note that the R_g parameter could not be determined (ND) for various species due to their lack of angular-dependence of scattered light.